# CHARACTERIZATION OF NONLINEAR DYNAMIC SOIL PROPERTIES FROM GEOTECHNICAL ARRAY DATA

S. F. Ghahari, and E. Taciroglu

Department of Civil & Environmental Engineering, University of California, Los Angeles

## Abstract

Dynamic soil properties are key ingredients of analyses for predicting/assessing soil-structure interaction (SSI) and site response effects under seismic excitations. While there is already a large amount of valuable data recorded by numerous geotechnical arrays worldwide, there is no reliable technique that enables the extraction of dynamic nonlinear/hysteretic properties of soil layers. Herein, a stochastic filtering method devised for estimating the nonlinear soil properties from earthquake data recorded by geotechnical arrays.1D-3C finite element site models are used, and the soil layers' constitutive model parameters and input excitation (bedrock or within motions) time-histories are identified using Unscented Kalman Filtering techniques. The method is first verified using synthetic examples and then validated using real-life data from centrifuge tests as well as the well-known Lotung site. Subsequently, the method is applied to earthquake data recorded by several CSMIP Geotechnical Arrays.

## Introduction

Although near-surface nonlinear soil layers have negligible dimensions compared to the path-lengths that seismic waves traverse from the source to the site, they significantly contribute to the observed motion at the ground surface [1]. Realistic physics-based predictions cannot be achieved unless they are the said nonlinearities are into account. While there are several veritable analytical and numerical methods to predict site-response given bedrock or outcrop motions (e.g., [2]–[4]), their accuracies inherently depend on the knowledge of the soil layers' dynamic properties. However, laboratory testing of "undisturbed" soil samples inevitably involves some violation of in-situ conditions. For example, loading paths in the laboratory tests are significantly different from those that the soil experiences in the field. Field measurements had been suggested to resolve this problem. Cross-Hole Tests (CHT), Down-Hole Tests (DHT), Suspension Logging, Seismic Reflection, Seismic Refraction, and Spectral Analysis of Surface Waves (SASW) are among various methods that are used for measuring shear wave velocities of soil layers, which is a key parameter for predicting the linear dynamic responses of a soil deposit. However, even these in-situ tests cannot mimic the site's actual behavior under real-life earthquakes because the sources of real-life seismic waves are inherently different from those used in in-situ tests. Moreover, in-situ tests are typically only able to capture the very-small-strain (and thus linear) soil layers' responses. On the other hand, it is well accepted that soil mostly behaves nonlinearly during even moderate earthquakes and reaches strains well beyond those that can be induced in conventional in-situ tests [5].

Not surprisingly, the estimation of dynamic site properties from recorded ground motions has been an important topic of research (for example, [6], [7]) because earthquakes may be regarded as prototype in-situ dynamic tests carried out by nature and the data recorded during earthquakes offer precious opportunities for the study of in-situ behavior of soil within a strain range that has engineering significance. However, most of the identification studies carried out in the past are limited to linear or equivalent linear soil properties of soil layers [8], [9]. These limited studies, in which soil nonlinearity was considered, have limited applicability because the assumed constitutive nonlinear model was very simple [10]. Moreover, in many of these studies, in-depth motions were used as input excitations through the conventional outcrop method (with absorbing boundary condition), which reduces the method's applicability range. More importantly, it is well accepted that within motions are polluted by down-going waves and should not be used as outcrop input excitations [11].

In this project, within a proposed general framework for nonlinear site characterization, which resolves all of the aforementioned limitations, we developed, tested, and validated input-output and output-only identification algorithms to estimate the nonlinear soil properties form data recorded in a geotechnical array. The proposed framework was verified using synthetic examples and validated using centrifuge data as well as real-life data recorded at the well-known Lotung site.

## The Proposed Framework

As schematically shown in Figure 1, the objective is to identify (*i*) the most plausible nonlinear constitutive model, (*ii*) parameters of the selected model, and (*iii*) the incident motion by using data recorded at several depths. A common simplifying assumption is also adopted—namely, the problem is an ideal 1D case with known layering and some relatively good initial but uncertain estimations of the parameters.

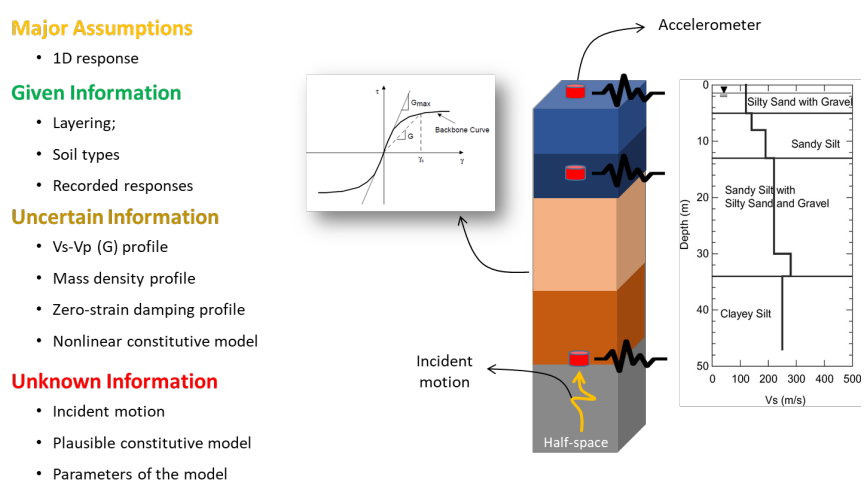


**Figure 1**. The proposed framework.

There are two approaches to carry out dynamic site response analyses, as shown in **Figure 2**. In the more traditional approach, the site is modeled up to the bedrock (half-space) level; and radiation damping is modeled by using an absorbing boundary to prevent wave

reflection. Through this approach, the incident motion must be used as input excitation, which can theoretically be obtained from the nearby rock outcrop motion (with a ½ factor). As seen, this approach is only valid if there is no impedance contrast below the boundary level, and there is a very close rock outcrop motion. In another approach, the domain can be cut at any depth as long as the so-called within motion is used as input excitation, and a fixed boundary is used.

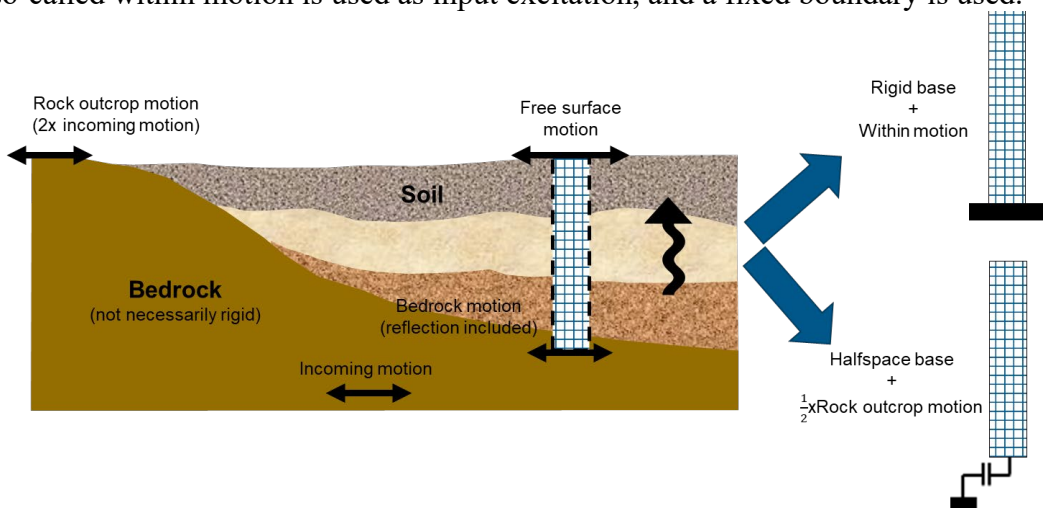


**Figure 2.** One-dimensional site response analysis approaches.

We propose to solve the inverse problem using output-only sequential Bayesian estimation [12], [13], as shown in **Figure 3**. In this approach, the 1D FE model of the site is modeled up to the bedrock depth with an absorbing boundary condition if the bedrock is not rigid. A soil constitutive model is chosen, and its parameters are identified along with the unknown incident motion through the Bayesian model updating. The entire process is then repeated using different constitutive models, and the most plausible and its optimal parameters are determined through classical model selection criteria [14], [15]. This joint input-parameter estimation solution will be later verified and validated through synthetic and centrifuge test data, respectively. It should be emphasized that input-output estimation can be employed if the bedrock is rigid, and there is a measurement at the bedrock depth to use as input excitation.

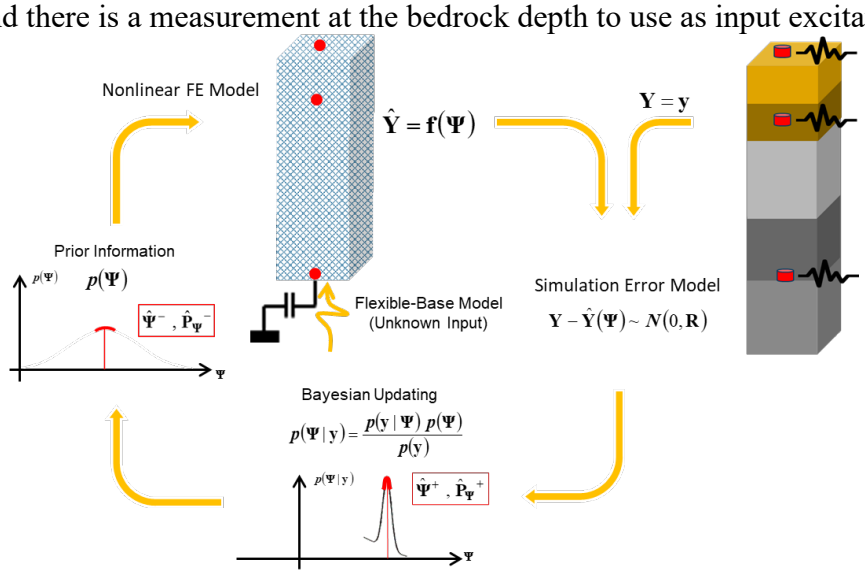


**Figure 3.** The one-step solution.

The aforementioned joint input-parameter estimation solution is prone to a high level of uncertainty if the number of parameters is large or the number of in-depth recorded data is limited. To resolve this issue, we solve the inverse problem in two sequential steps (see Figure 4). In Step 1, the 1D FE model of the site is fixed at the lowest instrumented level, such that the recorded within motions can be used as input excitation. A soil constitutive model is chosen, and its parameters are identified through the Bayesian model updating. Once completed the first step, the bedrock layer is added to the model in step 2 (through an absorbing boundary condition), and its parameters are estimated along with the incident motion, while the system above this level is known. Note that the first step can be limited to any depth as long as there is measured within motion at that depth. This is a crucial benefit, especially for the cases with deep bedrock level and only a few sensors at shallow depth for which properties of those shallow layers can be estimated with higher reliability. However, the model has to be extended up to the bedrock depth in the second step to be able to estimate incident motions too.

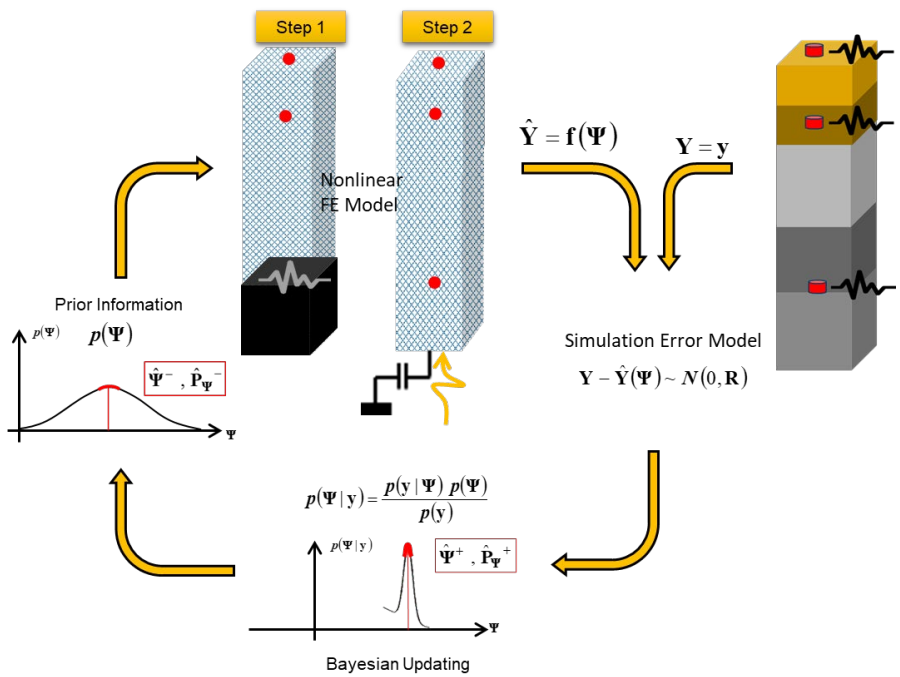


**Figure 4.** The two-step solution.

## The Bayesian Model Updating

Bayesian model updating is briefly reviewed for the readers' convenience. The formulation is presented for the general case of input-parameter estimation, while it is employed partially in Steps 1 and 2 as part of the two-step solution described above.

Let's assume a site with a soil deposit, as shown in Figure 5 (left). There are $m$ soil layers located above an elastic half-space with finite rigidity (bedrock) and excited by vertically propagating earthquake excitations. Absolute accelerations at several points (not necessarily at all layers or even boundaries of layers) are recorded by a geotechnical array. This continuous system can be modeled using a Finite Element (FE) model, as shown in Figure 5 (right) [16]. In this model, the soil is modeled in two-dimensions using plane strain elements. To account for the finite rigidity of the bedrock, a Lysmer-Kuhlemeyer [17] dashpot is incorporated at the base of

the soil column, whose coefficient equals the product of the mass density and shear wave velocity of the bedrock with the area of the base of the soil column (size of the element). The soil column is excited at the base by a horizontal force time-history, which is equal to the ground velocity multiplied by the dashpot's coefficient [18].

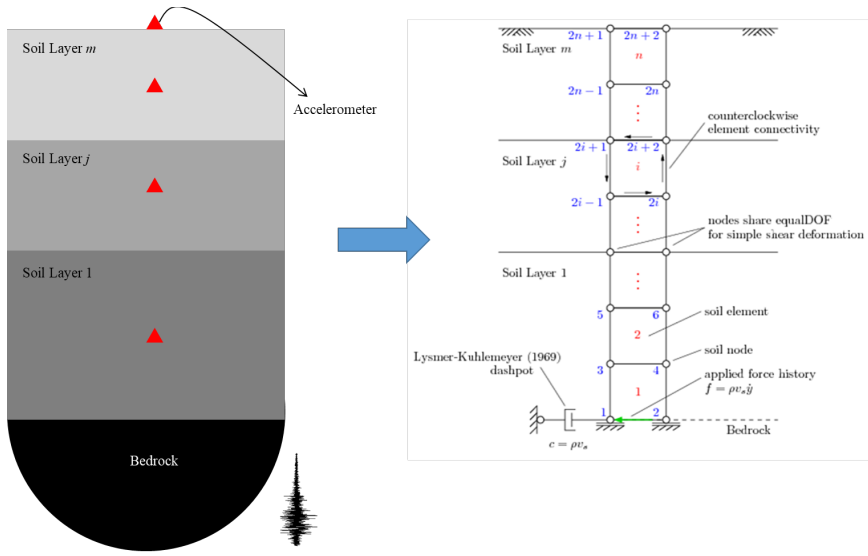


**Figure 5**. Instrumented soil deposit (left) and its equivalent discrete FE model (right).

The response of the FE model at each time step to the applied force time-history can be expressed as a nonlinear function of the model parameter vector, $\boldsymbol{\theta}$, and the time-history of the force, $\boldsymbol{f}_{1:i}$,

$$\hat{\boldsymbol{y}}_i = h_i(\boldsymbol{\theta}, \boldsymbol{f}_{1:i}), \tag{1}$$

where $\boldsymbol{\theta} = [\theta_1, \dots, \theta_{n_\theta}]$ contains $n_\theta$ parameters (e.g., the layers' shear wave velocities, parameters of the constitutive models, etc.) that define the FE model, and $h_i(.)$ is the nonlinear response function of the FE model at time step $i$, encapsulating all the dynamics of the model from time step 1 to $i$. The measured response vector of the site, $\boldsymbol{y}_i$, is related to the FE predicted response, $\hat{\boldsymbol{y}}_i$, as

$$\boldsymbol{v}_i(\boldsymbol{\theta}, \boldsymbol{f}_{1:i}) = \boldsymbol{y}_i - \hat{\boldsymbol{y}}_i(\boldsymbol{\theta}, \boldsymbol{f}_{1:i}), \tag{2}$$

where $\boldsymbol{v}_i \in \mathrm{R}^{n_y \times 1}$ is the simulation error vector that accounts for the misfit between the measured responses of the site at $n_y$ locations and the FE-predicted response. The simulation error is ideally modeled as a zero-mean Gaussian white noise vector (i.e., $\boldsymbol{v}_i \sim N(\mathbf{0}, \mathbf{R})$) by neglecting the effects of modeling error. The objective of the estimation problem is to find the estimates of the unknown parameter vector, i.e., $\boldsymbol{\psi}_i = \left[\boldsymbol{\theta}^T, \boldsymbol{f}_{1:i}{}^T\right]^T$, for which the discrepancies between the measured and FE predicted responses are minimized in a probabilistic sense. Since the estimation problem is highly nonlinear, a sequential estimation approach is used to improve estimation efficiency. In our approach, the time domain is divided into successive overlapping time windows, referred to as the estimation windows. The problem is then solved at each window to estimate the unknown parameter vector.

Assume that the $m$-th estimation window spans from time step $t_1^m$ to time step $t_2^m$. Therefore, the unknown parameter vector at this estimation window is defined as $\boldsymbol{\psi}_m = \left[\boldsymbol{\theta}^T, \boldsymbol{f}_{t_1^m:t_2^m}^{m\,T}\right]^T$, where $\boldsymbol{\psi}_m \in \mathrm{R}^{(n_{\boldsymbol{\theta}}+t_l)\times 1}$ , in which $t_l = t_2^m - t_1^m$ is the window length. The unknown parameter vector, $\boldsymbol{\psi}_m$, can be estimated using a parameter-only Kalman filtering method (e.g., [19]). To this end, the unknown parameter vector is modeled as a random vector, the evolution of which is characterized by a Gaussian Markov process—also known as a random walk. Then, a state-space model is set up, in which the state equation governs the evolution of the random parameter vector and the measurement equation corresponds to the discrepancies between the measured and FE predicted responses [20], i.e.,

$$\boldsymbol{\psi}_{m,k+1} = \boldsymbol{\psi}_{m,k} + \boldsymbol{\gamma}_{m,k}, \tag{3}$$

$$\boldsymbol{y}_{t_1^m:t_2^m} = \widehat{\boldsymbol{y}}_{t_1^m:t_2^m,k+1}\left(\boldsymbol{\psi}_{m,k+1}\right) + \boldsymbol{v}_{t_1^m:t_2^m,k+1}, \tag{4}$$

where $\boldsymbol{\gamma}_{m,k} \sim N(\mathbf{0}, \mathbf{Q})$, $\boldsymbol{v}_{t_1^m:t_2^m,k+1} \sim N(\mathbf{0}, \widetilde{\mathbf{R}})$, where $\widetilde{\mathbf{R}} \in \mathrm{R}^{(t_l\times n_y)\times(t_l\times n_y)}$ is a block diagonal matrix, whose block diagonals are the simulation error covariance matrix $\mathbf{R}$. In Eqs. (3) and (4), $k$ denotes the iteration number. As can be observed, the estimation process at each estimation window is iterative, i.e., the mean vector and covariance matrix of the unknown parameter vector is iteratively updated based on the discrepancies between the time histories of the measured and estimated responses.

An Unscented Kalman Filtering (UKF) [21] method can then be used to update the unknown parameter vector at each iteration. In our method, the nonlinear FE model is evaluated separately at a set of deterministically selected realizations of the unknown parameter vector, which are referred to as the sigma points (SPs) denoted by $\boldsymbol{\vartheta}^j$. The sigma points are selected around the prior mean estimate $\widehat{\boldsymbol{\psi}}^-$. In this study, a scaled Unscented Transformation (UT) based on $2n_{\boldsymbol{\psi}} + 1$ sigma points (i.e., $j = 1,2,\ldots,2n_{\boldsymbol{\psi}} + 1$) is used, where $n_{\boldsymbol{\psi}}$ denotes the size of the extended parameter vector. The mean and covariance matrix of the FE predicted structural responses, and the cross-covariance matrix of $\boldsymbol{\psi}$ and $\boldsymbol{y}$ are respectively computed using a weighted sampling method as

$$\overline{\boldsymbol{y}} = \sum_{j=1}^{2n_{\boldsymbol{\psi}}+1} W_m^j\, \widehat{\boldsymbol{y}}_i\left(\boldsymbol{\vartheta}^j\right), \tag{5}$$

$$\widehat{\mathbf{P}}_{\boldsymbol{yy}} = \sum_{j=1}^{2n_{\boldsymbol{\psi}}+1} W_e^j \left[\widehat{\boldsymbol{y}}_i\left(\boldsymbol{\vartheta}^j\right) - \overline{\boldsymbol{y}}\right]\left[\widehat{\boldsymbol{y}}_i\left(\boldsymbol{\vartheta}^j\right) - \overline{\boldsymbol{y}}\right]^T + \mathbf{R}, \tag{6}$$

$$\widehat{\mathbf{P}}_{\boldsymbol{\psi y}} = \sum_{j=1}^{2n_{\boldsymbol{\psi}}+1} W_e^j \left[\boldsymbol{\vartheta}^j - \widehat{\boldsymbol{\psi}}^-\right]\left[\widehat{\boldsymbol{y}}_i(\boldsymbol{\vartheta}^j) - \overline{\boldsymbol{y}}\right]^T, \tag{7}$$

where $W_m^j$ and $W_e^j$ denote weighting coefficients [21]. Now, the UKF prediction-correction procedure can be employed to estimate the posterior parameter mean vector $\widehat{\boldsymbol{\psi}}^+{}_{m,k+1}$ and covariance matrix $\widehat{\mathbf{P}}_{\boldsymbol{\psi},m,k+1}^+$ at each iteration. The proposed identification algorithm is summarized in Table 1.

**Table 1**. Identification algorithm for joint estimation of the model parameters and the FIM time history.

1. Set the estimation window length $t_l$, and the start and end points of each estimation window.
2. Set the initial mean vector and covariance matrix of the unknown parameter vector as
$$\widehat{\boldsymbol{\psi}}^{+}{}_{0} = \left[\widehat{\boldsymbol{\theta}}_0{}^{T}, \boldsymbol{f}^{0}_{t_1^0:t_2^0}{}^{T}\right]^{T}, \text{ and } \mathbf{P}^{+}_{\boldsymbol{\psi},0} = \begin{bmatrix} \widehat{\mathbf{P}}_{\boldsymbol{\theta\theta},0} & \mathbf{0} \\ \mathbf{0} & \widehat{\mathbf{P}}_{\boldsymbol{f}^0} \end{bmatrix}.$$
3. Define the process noise covariance matrix $\mathbf{Q}$ and the simulation error covariance matrix $\mathbf{R}$. Set up matrix $\widetilde{\mathbf{R}}$.
4. For the $m$-th estimation window:
   4.1. Retrieve the posterior estimates of the mean vector and covariance matrix of the unknown parameter vector from the last estimation window (i.e., $\widehat{\boldsymbol{\psi}}^{+}{}_{m-1}$, and $\mathbf{P}^{+}_{\boldsymbol{\psi},m-1}$). Set up $\widehat{\boldsymbol{\psi}}^{+}{}_{m,0}$ and $\mathbf{P}^{+}_{\boldsymbol{\psi},m,0}$ based on $\hat{\boldsymbol{\psi}}^{+}_{\boldsymbol{m}-1}$ and $\mathbf{P}^{+}_{\boldsymbol{\psi},m-1}$.
   4.2. Iterate ($k$ = 1, 2, …):
   a. Set $\widehat{\boldsymbol{\psi}}^{-}{}_{m,\mathrm{k}+1} = \widehat{\boldsymbol{\psi}}^{+}{}_{m,\mathrm{k}}$, $\mathbf{P}^{-}_{\boldsymbol{\psi},m,k+1} = \mathbf{P}^{+}_{\boldsymbol{\psi},m,k} + \mathbf{Q}$.
   b. Generate sigma points. Run the FE model for $(2n_{\boldsymbol{\psi}} + 1)$ sigma points. Derive $\overline{\boldsymbol{y}}$, $\widehat{\mathbf{P}}_{\boldsymbol{yy}}$, and $\widehat{\mathbf{P}}_{\boldsymbol{\psi y}}$ using Eqs. (5)-(7).
   c. Compute the Kalman gain matrix: $\mathbf{K} = \widehat{\mathbf{P}}_{\boldsymbol{\psi y}}\left(\widehat{\mathbf{P}}_{\boldsymbol{yy}}\right)^{-1}$.
   d. Find the corrected estimates of the mean vector and covariance matrix of the unknown parameter vector: $\widehat{\boldsymbol{\psi}}^{+}{}_{m,\mathrm{k}+1} = \widehat{\boldsymbol{\psi}}^{-}{}_{m,\mathrm{k}+1} + \mathbf{K}\left(\boldsymbol{y}_{t_1^m:t_2^m} - \overline{\boldsymbol{y}}\right)$, $\mathbf{P}^{+}_{\boldsymbol{\psi},m,k+1} = \mathbf{P}^{-}_{\boldsymbol{\psi},m,k+1} - \mathbf{K}\left(\widehat{\mathbf{P}}_{\boldsymbol{yy}} + \widetilde{\mathbf{R}}\right)\mathbf{K}^{T}$.
   e. Check for convergence: if $\left|\widehat{\boldsymbol{\psi}}^{+}{}_{m,k+1} - \widehat{\boldsymbol{\psi}}^{+}{}_{m,k}\right| < 0.02 \times \widehat{\boldsymbol{\psi}}^{+}{}_{m,k-1}$ or $k + 1 > 10$, then move to the next estimation window ($m = m + 1$, go to step 4); otherwise, iterate again at the current estimation window ($k = k + 1$, go to step 4.2).

## The Selected Constitutive Model

During the last few decades, a broad range of nonlinear soil models—uniaxial to multi-axial, phenomenological to physics-based—have been devised (e.g., [22], [23], [24], [25], [26]). For example, one of the most well-known and advanced nonlinear soil models is the one devised by Elgamal and co-workers [26]. In that model, soil plasticity is formulated based on the multi-surface concept, with a non-associative flow rule to reproduce the well-known dilatancy effect. The yield surfaces are of the Drucker-Prager [27] type. This model is frequently used in the direct simulation of SSI problems within the research community and is already available in OpenSees [28]. The multiple hierarchical yield surfaces of this model enable it to approximate the soil behavior within a broad range of strain regimes, but this is also its disadvantage in that a large number of requisite model parameters renders the calibration process formidable. By the same token, the model may exhibit spurious sensitivities. As we are going to solve a massive inverse problem using real-life data, these two major drawbacks are problematic.

A model with a simpler scaffold is that proposed by Borja and Amies [23]. This is also a multi-surface model but it only has a bounding surface and a vanishing elastic region. Incidentally, the Borja-Amies (BA) model only needs a few parameters for calibration. The validity of this model was examined by utilizing the downhole array motions recorded at Lotung, Taiwan, through one-dimensional nonlinear site response analyses [29] with promising success. The model admits an additive decomposition of the stress into inviscid (frictional) and viscous parts, as in:

$$\boldsymbol{\sigma} = \boldsymbol{\sigma}^{inv} + \boldsymbol{\sigma}^{vis}, \quad \boldsymbol{\sigma}^{inv} = \boldsymbol{C}^{e}:(\boldsymbol{\epsilon} - \boldsymbol{\epsilon}^{p}), \quad \boldsymbol{\sigma}^{vis} = \boldsymbol{D}:\dot{\boldsymbol{\epsilon}} \tag{8}$$

where $\boldsymbol{C}^e$ and $\boldsymbol{D}$ are elastic stiffness and viscous damping tensors, respectively; $\boldsymbol{\epsilon}$ is the total strain tensor; $\boldsymbol{\epsilon}^p$ is the plastic strain tensor; and $\dot{\boldsymbol{\epsilon}}$ is the total strain rate. Given this decomposition, the model can also incorporate material level strain-rate-dependent damping, which enables a modeler to match field-identified damping behavior, even when such behavior is complex. Omitting details here for brevity, the main equation to calibrate this model is,

$$\frac{G}{G_{max}} = 1 - \frac{3}{2\tau_o}\int_0^{2\tau_o}\left[h\left(\frac{R/\sqrt{2}+\tau_o-\tau}{\tau}\right)^m + H_0\right]^{-1} d\tau \tag{9}$$

where $G = \tau_o/\gamma_o$ is the secant shear stiffness, and $R$ is the radius of the bounding surface, and parameters $h$, $m$ and $H_0$ control the intensity of the hardening. The model can be directly calibrated using an experimentally obtained (or otherwise estimated from real-life) $G/G_{\max}$ curve [30] and a frequency-dependent damping curve. In the present study, we will explore the capabilities of this soil model in capturing the dynamic response of soils, and we will incorporate it with the UKF-based estimation method we have described above.

The advantages of the BA model are clear:

- It is a thermodynamically consistent model based on the classical viscoplasticity framework with well-defined parameters.
- It is a three-dimensional model, and thus, if it is accurately calibrated, it can accurately predict soil behavior under multi-axial stress states, such as those due to irregular surface topography and soil stratigraphy, or underground scatterers.

As a part of a parallel study, the BA model has been successfully implemented in OpenSees and extensively verified and validated [31]. In this study, we use OpenSees [28] for all needed simulations, and the soil model is this recently implemented BA model.

## Verification

### Proof-Of-Concept Study

To verify the single-step joint input-parameter estimation solution, we synthetically generated the acceleration response of a 4-layer soil deposit on top of bedrock, as shown in Figure 6. To show that the estimation solution can work regardless of the material model, pressure-dependent elastic-plastic behavior is considered for the soil wherein plasticity is formulated based on the multi-surface concept with a non-associative flow rule to reproduce the dilatancy effect [26]. This model is already implemented in OpenSees [28]. The most important parameters needed to create this model are shown in Figure 6 for reproducibility. A Rayleigh damping matrix is considered, which generates low strain damping ratios of 2% at 0.2 and 20 Hz. The model is excited by the ground motion shown on the bottom-right of Figure 6, which is recorded by the Gilroy #1 array; and the site response (accelerations) is measured at five below-ground locations.

Since the numerical accuracy of the wave transmission is known to be affected by both the frequency content of the input and the propagation wave-speed characteristics of the domain, the spatial element size was considered to be one-tenth of the smallest wavelength [32]. By

limiting the frequency of interest to 20 Hz and by assuming a minimum shear wave velocity of 40 m/s (much lower than available values), the element size of 0.2 m was used in this example. As this is an inverse problem, we used uniform meshing in-depth, while a finer mesh could be used in layers with higher shear wave velocities. Also, while the sampling rate is kept at 200 Hz in the analyses for the accuracy of the direct integration method, the highest reliable frequency would be 20 Hz.

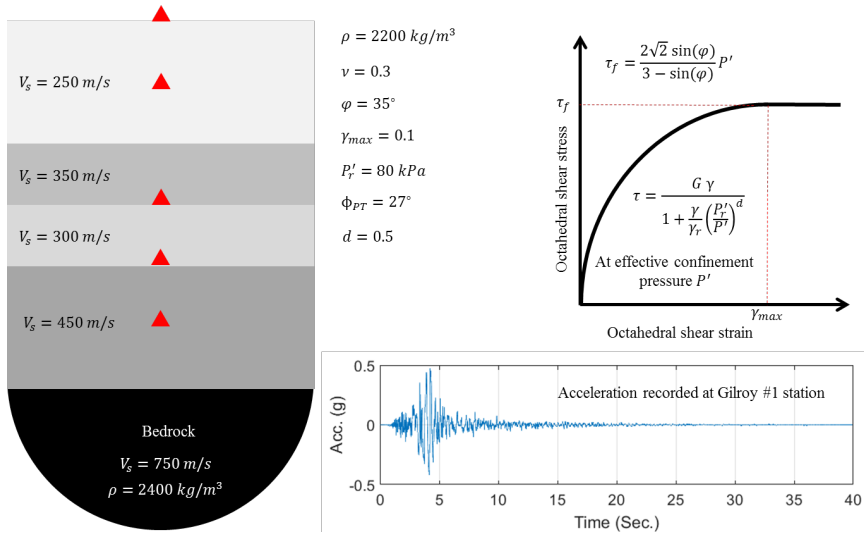


**Figure** 6. An illustrative example.

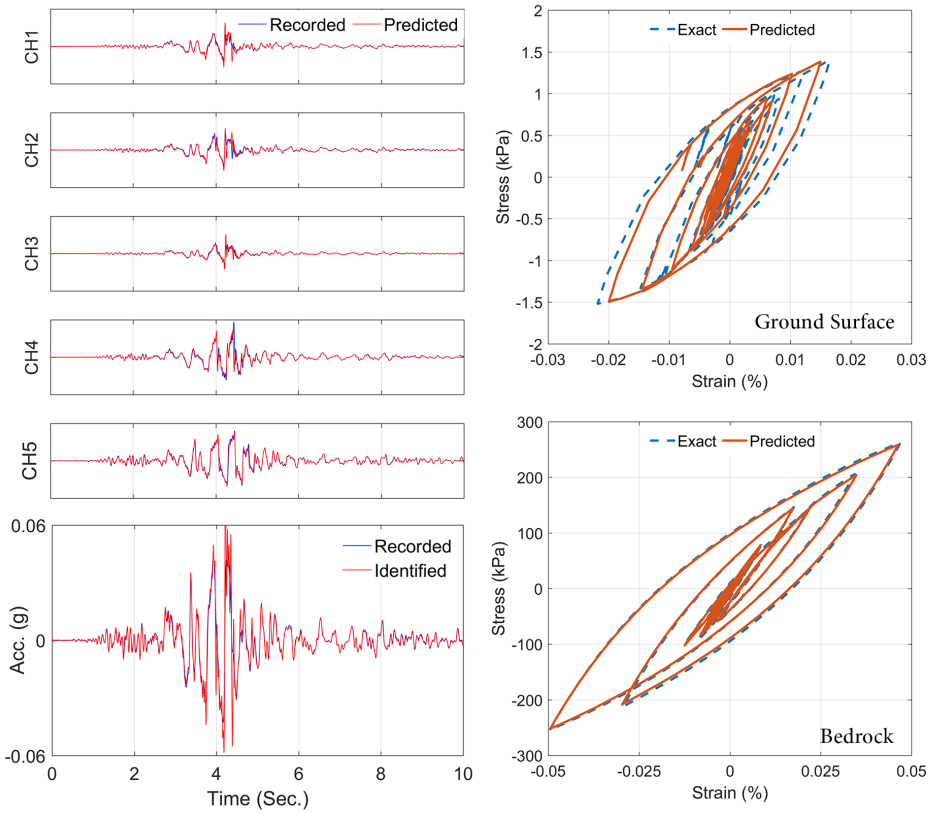


**Figure 7.** Identification results. Recorded and predicted responses (top-left), exact and identified bedrock acceleration (bottom-left), and Hysteresis loops near the surface and near the bedrock (right).

The input force (i.e., bedrock velocity time history), the shear wave velocities at three top layers, the pressure-dependency coefficient ($d$), and low-strain damping are assumed as unknown parameters and are estimated through the proposed output-only estimation method. We only used 10 seconds of the signals for the estimation and ran the algorithm in consecutive 2.5-second windows with a 1-second overlap. We assumed a 50% initial error for the unknown parameters. The identification results are shown in Figure 7. As seen, the bedrock acceleration, site response at the instrumented locations, as well as hysteresis loops near the surface and the bedrock are identified with very good accuracy (no stress/strain data was used for the identification). Results show that all of the unknown parameters, except the damping value, are estimated with final errors that are less than 3%. The damping value was not accurately identified because it does not significantly change the site response as seen in Figure 7. The sensitivity of the measured response with respect to the model parameters (parameter identifiability) needs an in-depth identifiability study which will be discussed later.

## The Lotung Site

To verify the proposed inverse solution, the Lotung site is simulated which will be later used for the validation studies too. Therefore, this site and its data are briefly reviewed here.

The Lotung Large-Scale Seismic Tests (LSST) site is located in the North-East of Taiwan. This site was established in a seismically active region in 1985 to study seismic soil-structure interactions effects on nuclear power plants. To do so, two scaled structures were constructed by the Electric Power Research Institute (EPRI) and the Taiwan Power Company [33]. In addition to the structures, the responses of the soil were recorded in several locations on the surface, and at different depths, as shown in Figure 8. Due to such dense instrumentation, the data from this site has been the subject of many studies [29], [34]–[38]. Specifically, Zeghal and Elgamal [7], [39] have extensively studied several earthquake data sets recorded at this site between 1985 to 1986 (Table 2)[1].

Out of these 18 events, the first three events and Event No. 13 are not available. Also, the digitized signals' resolution is relatively poor in several cases (Events No. 5, 6, 8, 9, 10, 15, 17, and 18). We also need data with a significant level of motion to observe soil nonlinearity. Moreover, the site's behavior must be close to 1D, so the source of the earthquake should be far from the site. Considering these criteria, events 7 and 16 are the best candidates that have been used by Borja et al. [29], [38], [40] too. The channels mostly used in previous studies and used here are FA1-5, DHB6, DHB11, DHB17, and DHB47 (see Figure 8) which are at depths of 0, 6, 11, 17, and 47 meters, respectively. It is noteworthy that Channel 47 is not available in Event No. 16, so Step 1 (Input-Output identification) can only be carried out for the first 17 meters.

[1] Data is publicly available at http://soilquake.net/Downholearray/Lotung/

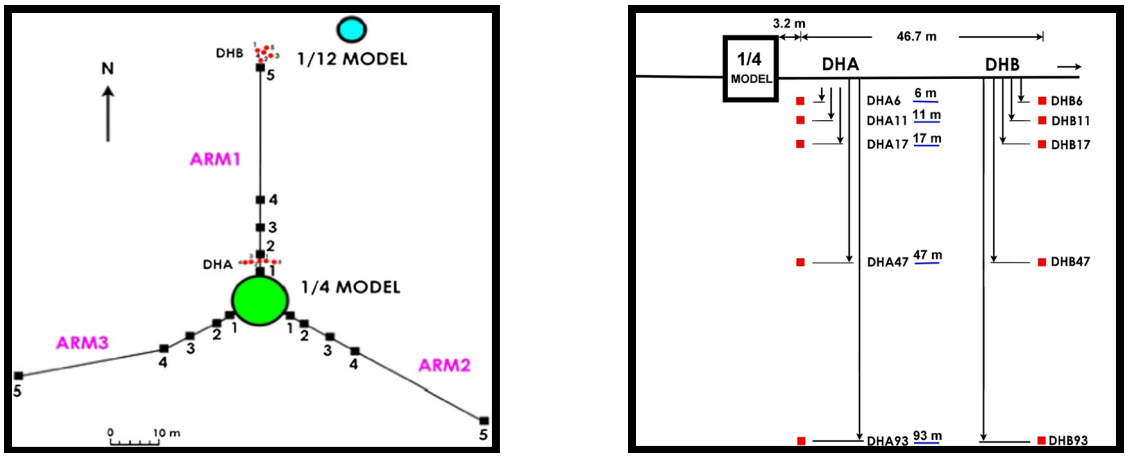


**Figure 8**. Plan (left) and elevation (right) views of the Lotung site.

**Table 2**. Recorded earthquake data at the Lotung site [7], [41].

| Event (1) | Date (2) | Magnitude ($M_l$) (3) | Epicentral distance (km) (4) | Focal depth (km) (5) | Distance to zone of energy release (km) (6) | Peak Acceleration[a] EW (g) (7) | NS (g) (8) | V (g) (9) |
|---|---|---|---|---|---|---|---|---|
| LSST 1 | 9/20/85 | — | — | — | — | —[b] | — | — |
| LSST 2 | 10/26/85 | 5.3 | — | — | — | 0.03 | 0.03 | 0.01 |
| LSST 3 | 11/7/85 | 5.5 | — | — | — | 0.01 | 0.01 | 0.01 |
| LSST 4 | 1/16/86 | 6.5 | 23.7 | 10.2 | 25.80 | 0.15[c] | 0.26[c] | 0.11[c] |
| LSST 5 | 3/29/86 | — | — | — | — | 0.04 | 0.03 | 0.03 |
| LSST 6 | 4/8/86 | 5.4 | 31.4 | 10.9 | 33.24 | 0.04 | 0.03 | 0.01 |
| LSST 7 | 5/20/86 | 6.5 | 66.2 | 15.8 | 68.06 | 0.16 | 0.21 | 0.04 |
| LSST 8 | 5/20/86 | 6.2 | 69.2 | 21.8 | 72.55 | 0.03 | 0.03 | 0.01 |
| LSST 9 | 7/11/86 | 4.5 | 5.0 | 1.1 | 5.12 | 0.07 | 0.05 | 0.01 |
| LSST 10 | 7/16/86 | 4.5 | 6.1 | 0.9 | 6.17 | 0.03 | 0.04 | 0.02 |
| LSST 11 | 7/17/86 | 5.0 | 6.0 | 2.0 | 6.32 | 0.07 | 0.10 | 0.04 |
| LSST 12 | 7/30/86 | 6.2 | 5.2 | 1.6 | 5.44 | 0.16 | 0.19 | 0.20 |
| LSST 13 | 7/30/86 | 6.2 | — | — | — | 0.05 | 0.03 | 0.02 |
| LSST 14 | 8/5/86 | 4.9 | 4.7 | 2.3 | 5.32 | 0.05 | 0.03 | 0.02 |
| LSST 15 | 11/14/86 | — | — | — | — | 0.02 | 0.04 | 0.05 |
| LSST 16 | 11/14/86 | 7.0 | 77.9 | 6.9 | 78.21 | 0.13 | 0.17 | 0.10 |
| LSST 17 | 11/14/86 | — | — | — | — | 0.04 | 0.04 | 0.02 |
| LSST 18 | 11/15/86 | — | — | — | — | 0.03 | 0.02 | 0.01 |

[a]Peak accelerations for the DHB array including the surface FA1-5 station.
[b]LSST 1 records did not include any free field motion.
[c]LSST 4 records were affected by electric glitches.

As the BA model is being used in this study, we model the Lotung site using the information provided by Borja et al. [29], [38]. Figure 9 shows the layered FE model of the first 47 m of the Lotung site with a fixed bottom condition (within boundary condition) and the shear wave velocity and elastic shear modulus profiles. The instrumented depths are specified by red circles (the lowest level is at the fixed boundary). The parameters of the BA model for all layers are the same and taken from [40] as $R = 0.0015G_{max}, H_0 = 0, h = 0.63G_{max}, m = 0.97$ and the Poission ratio is 0.48. The fundamental natural frequency of the elastic model that is fixed at 47m-depth is 1.33 Hz. Note that this frequency could be different from the natural frequency of the Lotung site. The natural frequency of the model is obtained by applying a fictitious fixed boundary condition (imposing an infinite impedance contrast), but the dominant frequency observed in the recorded data could be different depending to the depth at which there is actually such significant impedance contrast [42].

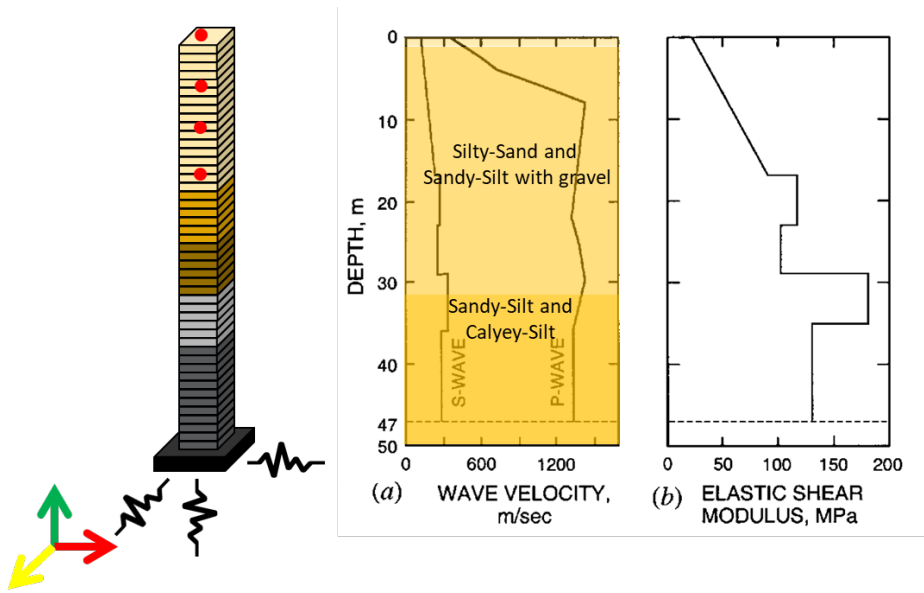


**Figure 9**. The FE model of the first 47 m of the Lotung site with a fixed bottom condition (left) and shear wave velocity and elastic shear modulus profile (right) [40].

To set the damping parameters, Borja et al. [40] identified a dominant excitation frequency of 0.65 Hz from the recorded signal at a depth of 47 m in the LSST7 event. They assumed a 1% stiffness proportional damping resulting in a factor of 0.005. So, the same level of damping was assumed in this study whenever simulations are carried out. To make the results comparable, the same modeling and analysis assumptions are used. An element size of 1 m is used through which frequencies up to 25 Hz can be resolved. So, all recorded signals are decimated to 50 Hz. Analyses are also carried out at the same rate, but subsampling is used whenever there is a convergence issue. Similar to [40], the Hilber-Hughes-Taylor (HHT) integration method with $\alpha = -0.1, \beta = 0.3025$, and $\gamma = 0.6$ is employed for all analyses. The effect of pore water pressure is neglected and all analyses are carried out in a total stress state.

### *Verification Studies*

As mentioned earlier, the first step of the proposed two-step solution can be carried out for any depth as long as there is a sensor at that depth to record the "within motion." So, we present results for the first 17 m because there is a large gap between this depth and 47 m.

As shown before (see Figure 9), the modulus of elasticity increases linearly in the first 17 m. So, the parameters $P_1$ to $P_9$ are considered as candidate updating parameters to represent the soil properties using the following definitions:

$$G_{max} = P_1 + zP_2 \tag{10}$$

$$\nu = P_3 \tag{11}$$

$$S_u = P_4 + zP_5 \tag{12}$$

$$h = P_6 + zP_7 \tag{13}$$

$$m = P_8 \tag{14}$$

$$a_1 = P_9 \tag{15}$$

where $z$ is the depth from the ground surface and $S_u$ is undrained shear strength. An identifiability study [43] is first carried out using LSST7 simulation data to find out which parameters are identifiable. Figure 10(left) shows the entropy gain of these 9 parameters. As seen, the Poisson's ratio is unidentifiable (at least around the assumed value), while the other 8 parameters are identifiable. However, there are two important notes: 1- the identifiability here means the responses are sensitive to the variation of these parameters, but the results of the identification could be sensitive to the start point, as the problem is not convex. 2- There is no absolute threshold above which parameters are guaranteed to be identifiable. Indeed, this index can only detect the identifiability of parameters with respect to each other. Another fact that can reduce the identifiability of the parameters is their mutual correlation. Figure 10(right) shows the severity of this correlation among these nine parameters (scaled to their entropy to be comparable). As seen, the only significant correlation is between parameters defining depth variation of $S_u$ and $h$. That is, $S_u$ and $h$ might not be properly identified.

Figure 11 shows how the identification algorithm performs having 8 unknown parameters (the Poisson ratio is excluded) and using simulated data from LSST7 event. We started the identification assuming a 50% initial error. As seen, while the predicted responses are perfectly matched to the recorded (here simulated) responses, some parameters are not identified very well due to the observed cross-correlation in the identifiability results.

We repeated the same problem with depth invariant parameters in simulation and identification, i.e., $G_{max} = P_1$, $S_u = P_4$, $h = P_6$, $m = P_8$, and $a_1 = P_9$. As shown in Figure 12, this is a healthy identification problem because there is no information sharing among parameters, so all five parameters are identified with an acceptable level of accuracy.

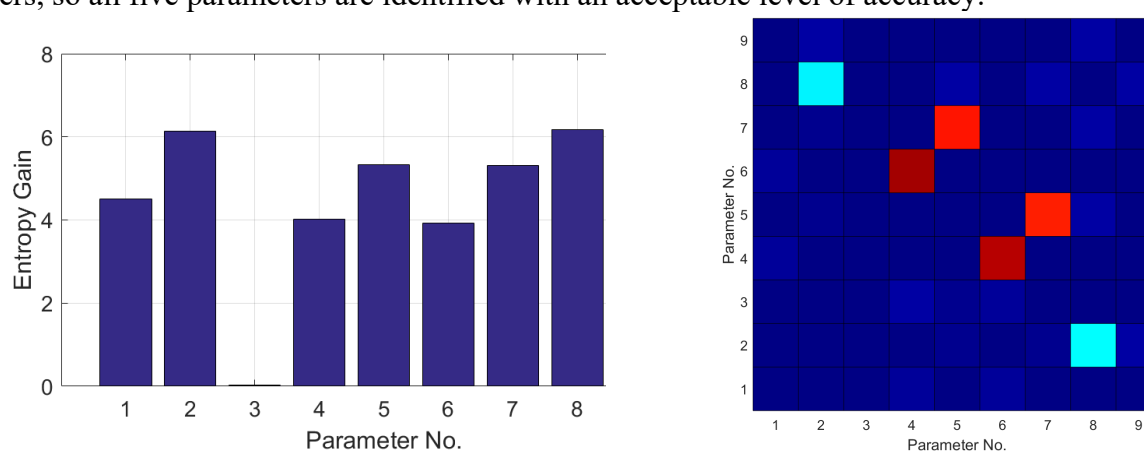


**Figure 10**. The identifiability study: entropy gain of each parameter (left), and the mutual information (right).

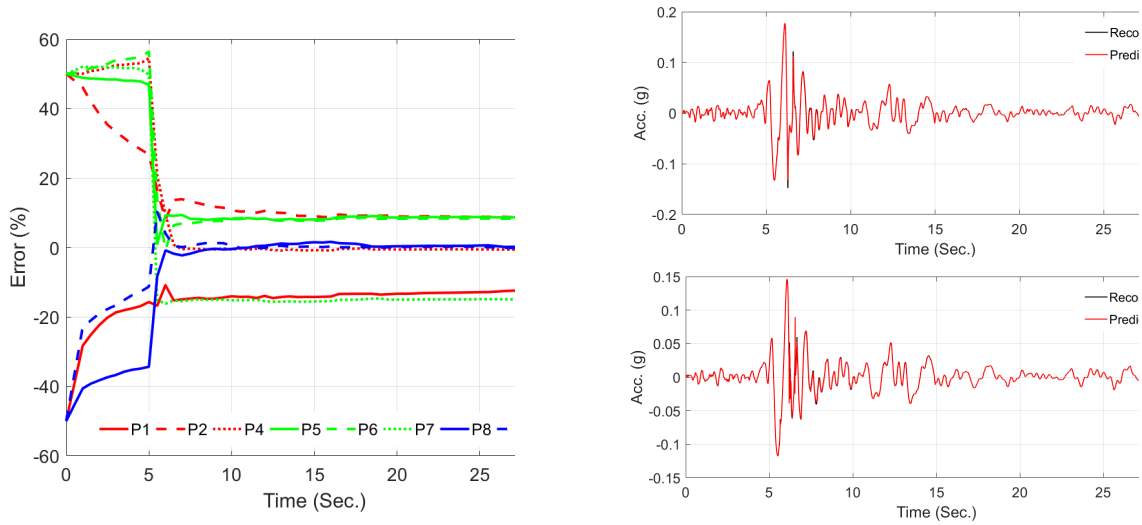


**Figure 11**. The identification results using 8 parameters. Left: identification progress, right: comparison between recorded (simulated) and predicted responses in the EW direction at the ground surface and depth 6m.

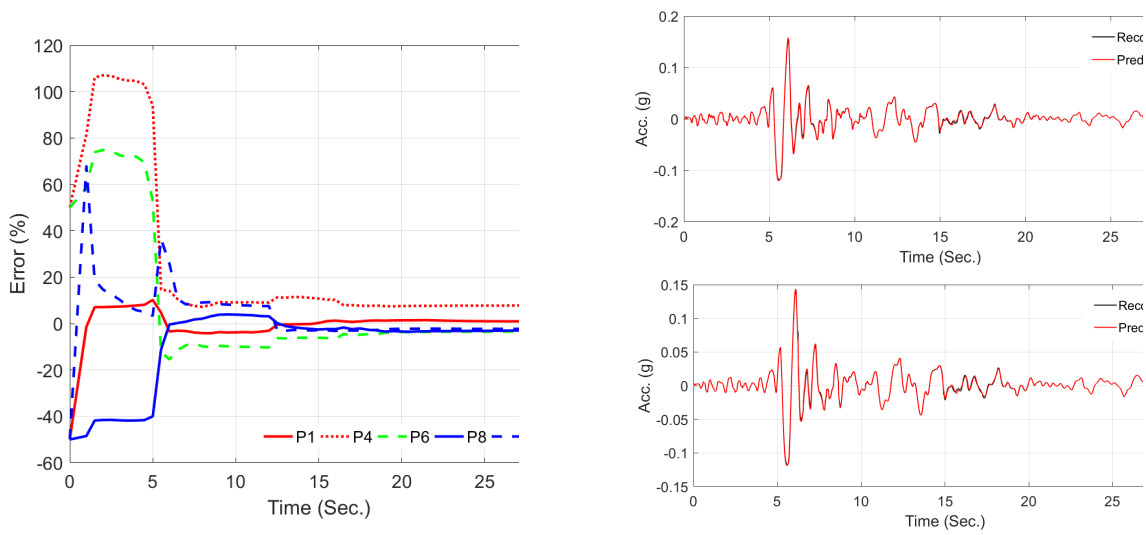


**Figure 12**. The identification results using 5 parameters. Left: identification progress, right: comparison between recorded (simulated) and predicted responses in the EW direction at the ground surface and depth 6m.

## Validation

### The Earthquake Data of The Lotung Site

Having a good understanding of the parameters' identifiability and the algorithm's performance, we use the real data from the LSST16 event to validate the estimation method. This event was selected because the behavior of the site is more close to 1D due to the long distance to the earthquake source [38]. We carry out the identification using two sets of updating parameters. In the first case, we use the same set of 8 parameters used in the simulated case

study, and we start the identification using the values suggested in [38]. Figure 13(left) shows how the parameters change in time when different time windows of data are received by the identification algorithm. The comparison between recorded, initial, and updated responses in Figure 14(left) shows that the updated model can predict responses, 22%, 15%, and 13% more accurately than the initial model in the EW-direction, respectively. By fixing the shear strength and consequently reducing the number of parameters, the accuracy of the updated model is even higher as shown in Figure 14(right). The percentage numbers are 27%, 19%, and 16%, respectively, in this case.

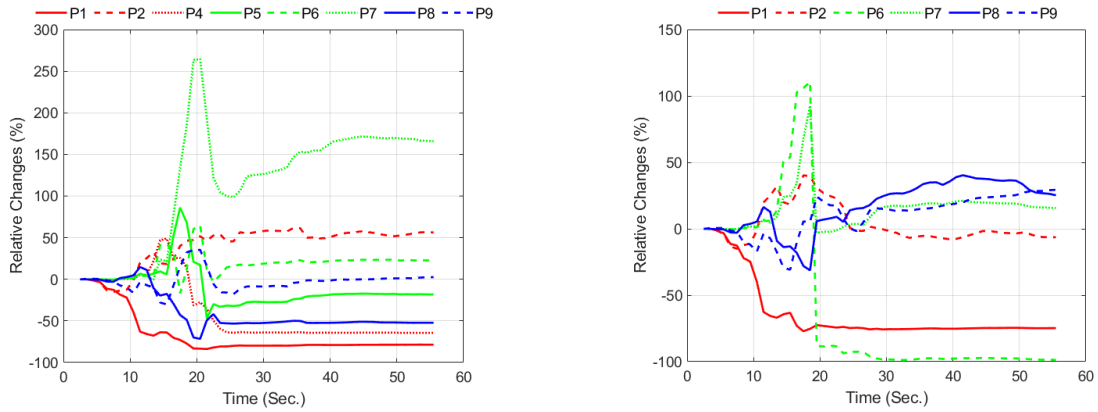


**Figure 13**. The identification results using two different parameter sets.

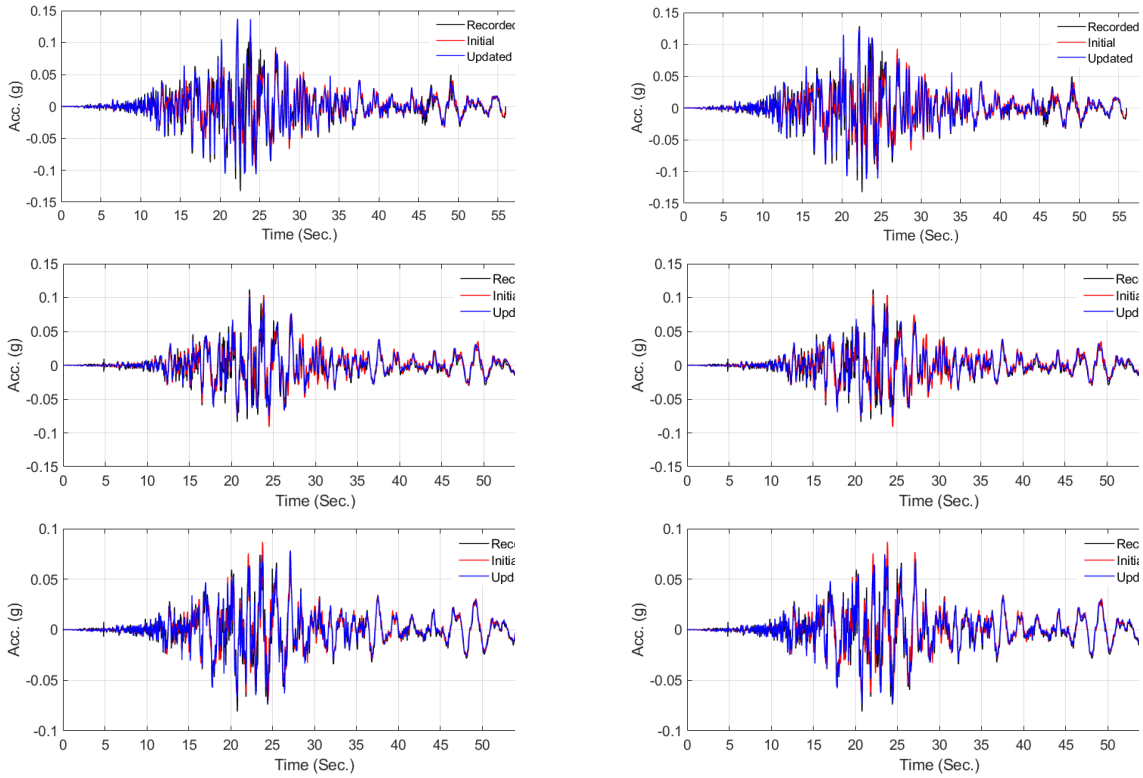


**Figure 14**. Comparison between recorded, initial, and updated responses using two different sets of parameters. The plots from top to bottom are responses at the ground surface to a depth of 11 m, respectively.

## The Centrifuge Test Data

The centrifuge test data is precious data for the validation studies because parameters of the domain and input excitations are largely under control. Herein, we use data from a very recent centrifuge test series on buried culvert structures. The configuration of the test and the types of input excitations used to excite the domain are shown in Figure 15. The details of these tests can be found in [44]. The data from the free-field column (far from structures) under Event #10 is used here. The 1D-3C FE model, the sensor location, and the parameters of the BA model, which are obtained from [45], are shown in Figure 15 too. Assuming these values as exact parameters, the simulated responses at 5 instrumented elevations under Motion #10 are compared with the recorded signals in Figure 16. The simulation was carried out in both OpenSees and Abaqus for further verification of the OpenSees BA implementation. As seen, the model can simulate the response very well.

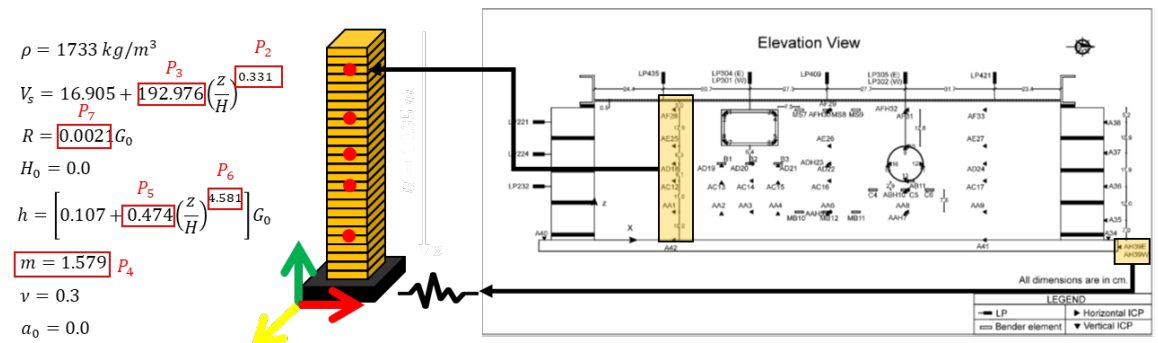


| Earthquake | Year | Station | Component | Magnitude | $R_{jb}$ (km) | $V_{s30}$ (m/s) |
|---|---|---|---|---|---|---|
| Northridge | 1994 | Beverly Hills | MUL279 | 6.69 | 9.44 | 355.81 |
| Northridge | 1994 | Santa Monica City Hall | STM090 | 6.69 | 17.28 | 336.20 |
| Hector Mine | 1999 | Hector | HEC000 | 7.13 | 10.35 | 726.00 |

| Event # | Command input type | Amp. factor applied to target motion |
|---|---|---|
| 1 | Step function | 0.6 |
| 2 | Step function | 1.5 |
| 3 | Earthquake MUL279 | 0.1 |
| 4 | Earthquake SMT090 | 0.1 |
| 5 | Earthquake HEC000 | 0.33 |
| 6 | Earthquake MUL279 | 0.5 |
| 7 | Earthquake SMT090 | 0.5 |
| 8 | Earthquake HEC000 | 1 |
| 9 | Earthquake MUL279 | 1 |
| 10 | Earthquake SMT090 | 1 |
| 11 | Earthquake HEC000 | 3 |

**Figure 15**. Centrifuge experiment.

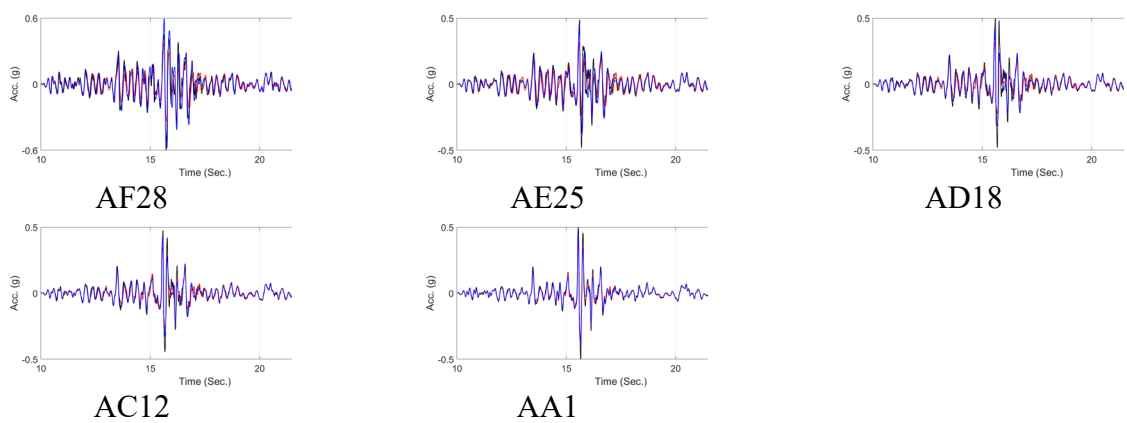


**Figure 16**. Forward simulation using assumed considered exact values.

We use this model and data to validate the single-step solution, as the model is physically fixed at the base. The base motion along with seven parameters specified in Figure 15 are considered as unknown parameters. We start the updating assuming a 50% initial error for the

parameters and 10% initial Coefficient Of Variation (COV). The results of the identification are shown in Table 3. As seen, out of these 7 parameters, Parameter 3 has a very large estimation COV showing that the problem is almost insensitive to this parameter, and the estimated value is unreliable. All other parameters are estimated with small COV, and the estimated values are reliable, and most of them are close to the considered exact values with various differences. However, Parameter 5 shows a very large difference with respect to the considered exact value. To see how the predicted responses using these values differ from Figure 17 is presented. In this figure, the comparison between recorded and predicted using the estimated parameters are shown on the right side, while the previous simulations are shown on the left side. As seen, the responses obtained from the updated model are closer to the recorded responses. As these responses are used for the model updating, it is not surprising to see such better prediction, but as shown in Figure 18, the estimated input excitation is very close to the recorded motion at the base of the shake table, confirming the results of the output-only model updating is very reliable.

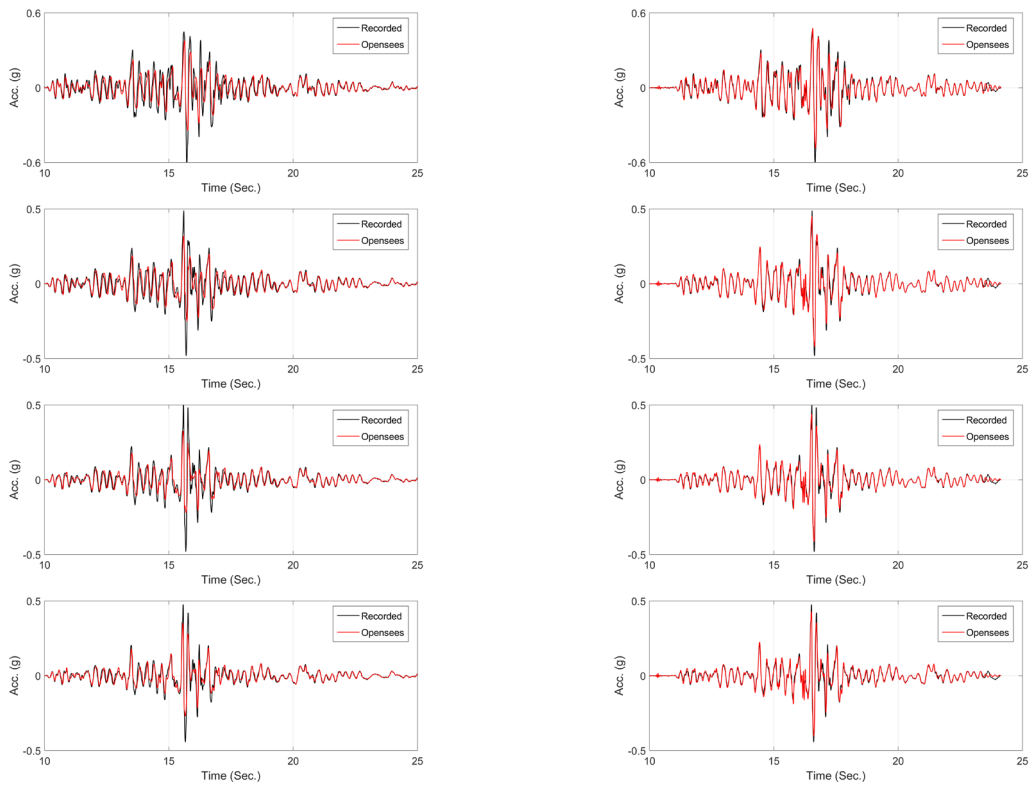


**Figure 17**. Comparison between recorded and predicted acceleration responses at four top sensors using considered exact (left) and identified (right) parameters.

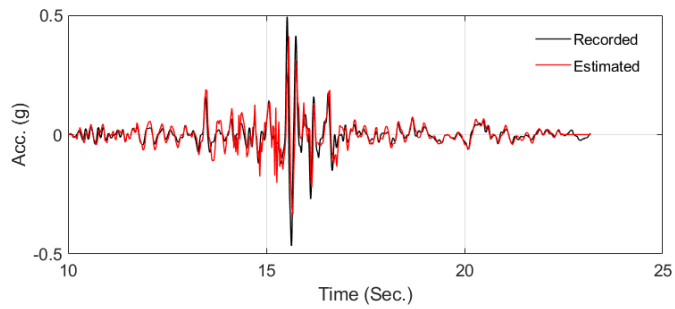


**Figure 18**. Comparison between exact and estimated input excitations.

**Table 3**. identification results.

| Parameter | Initial Value | Final Value | Initial COV | Final COV |
|---|---|---|---|---|
| 1 | +50% | -1.4% | 10% | 0.0% |
| 2 | +50% | +91% | 10% | 0.2% |
| 3 | +50% | +50% | 10% | 70% |
| 4 | +50% | +7% | 10% | 1.0% |
| 5 | +50% | +800% | 10% | 3.2% |
| 6 | +50% | -33% | 10% | 2% |
| 7 | +50% | -13% | 10% | 0.0% |

## Application to CSMIP Geotechnical Arrays

As a real-life application, the data from the CSMIP station 68323 is used. Figure 19(left) shows the instrumentation layout and the P- and S-wave velocity profiles. The idealized version of the $V_s$ profile was taken from [46] as shown in Figure 19(right). this idealized profile was later more idealized into 6 layers as colored in Figure 19(right). By the time of this study, 8 earthquake events have been recorded by this station, which are all very weak motions. The largest event is the 2014 South Napa event in which Peak Ground Acceleration (at the surface) was about 0.03g.

The $V_s$ profile below 35 m is unknown, so we only carry out the first step (input-output) identification. Figure 20 shows the comparison between the predicted responses using the updated model and the recorded signals. The comparison between the updated Vs profile and the initial and modified profiles are shown in Figure 21. The modified profile is the idealized version of the initial profile as shown in Figure 19(right).

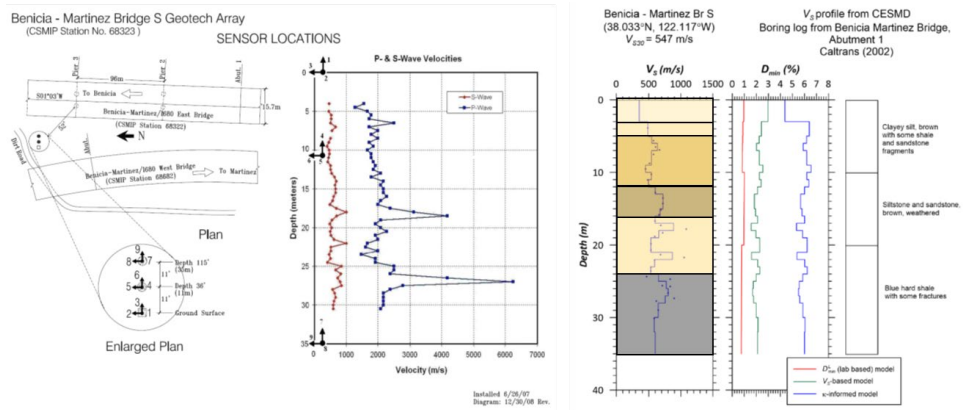


**Figure 19**. Benicia-Martinez Geotechnical Array. Instrumentation layout from CESMD (left), shear wave velocity, and small-strain damping profile.

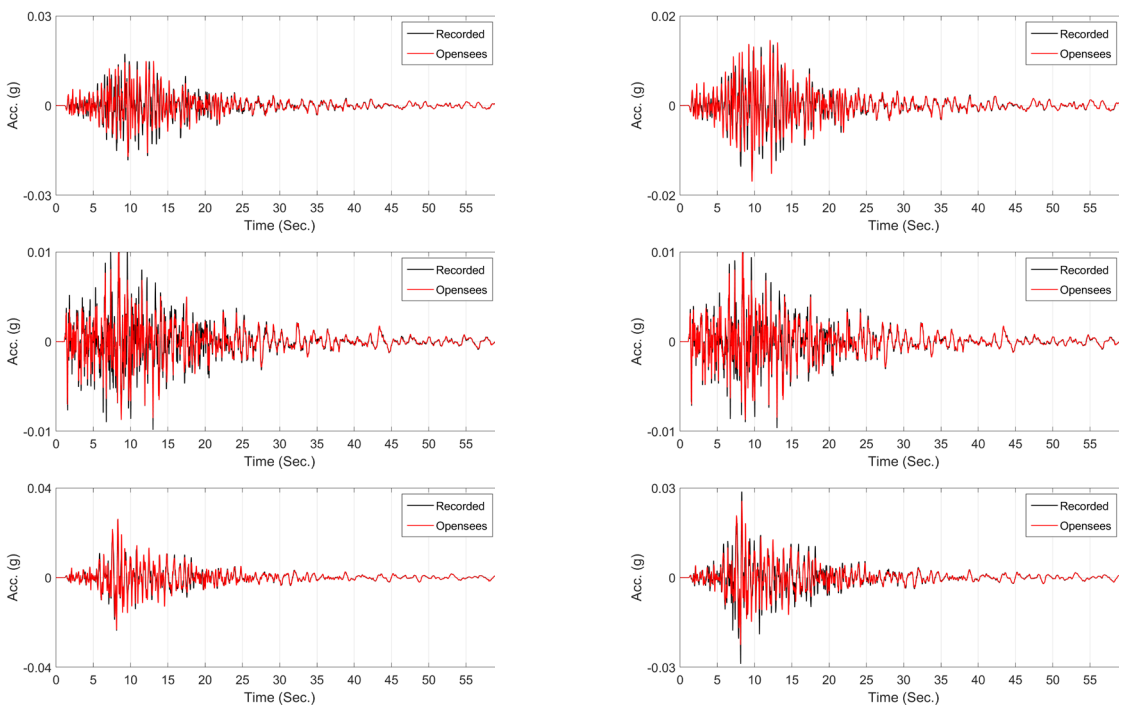


Ground surface Depth 11 m

**Figure 20**. Comparison between recorded and predicted responses in the South Napa 2014 earthquake. Plots from top to bottom show NS, vertical, and EW directions.

To see how this updated model works under another earthquake event, we carried out a blind prediction under El Cerrito 2010 event. Figure 22 shows a comparison between recorded and predicted ground surface motions using initial(modified) and updated models. As seen, the updated model can predict the ground surface more accurately.

Several other CSMIP stations were also studied using the proposed method. The results of those cases will be presented in the final report of the project.

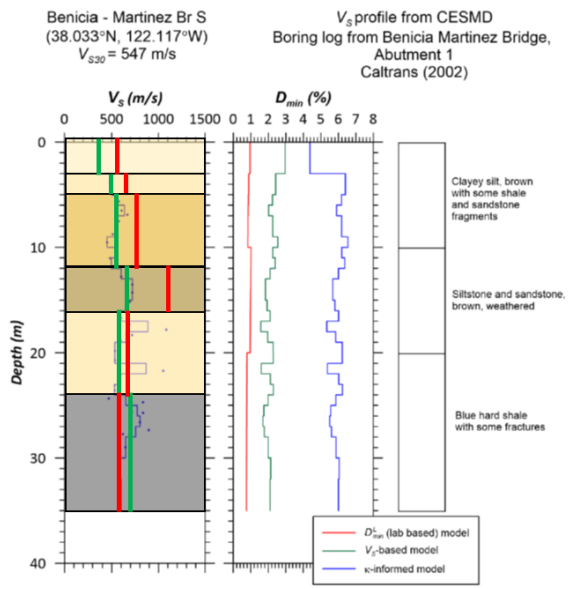


**Figure 21**. Comparison between initial, modified, and updated $V_s$ profile.

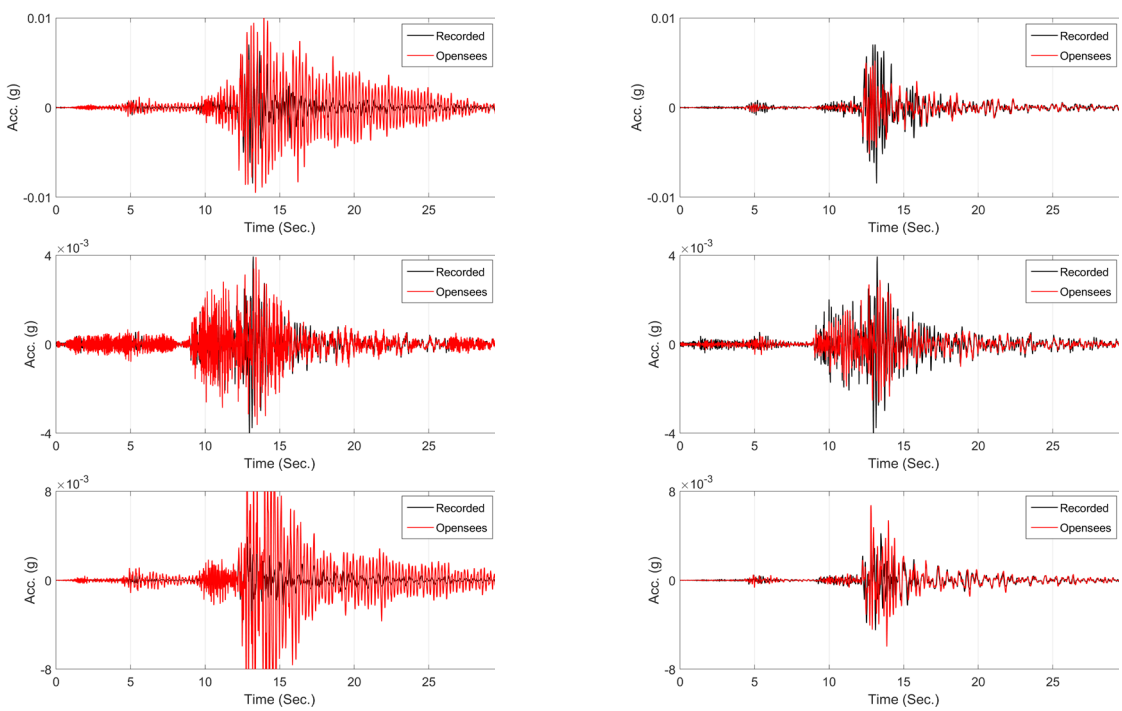


Initial(modified) model Updated model

**Figure 22**. Comparison between recorded and predicted ground surface responses in the El Cerrito 2010 earthquake. Plots from top to bottom show NS, vertical, and EW directions.

## Conclusions

Dynamic soil properties are key ingredients of analysis for predicting/assessing soil-structure interaction (SSI) and site response effects under seismic excitations. Although there are various techniques and tools to carry out forward site response analysis with various complexity

levels, there could be significant uncertainty due to the available uncertainties in nonlinear soil models and their parameters. In this project, we developed, tested, and validated input-output and output-only identification algorithms to estimate nonlinear soil properties from data recorded in the geotechnical array. The method was verified using synthetic examples and validated using centrifuge data and data recorded in the well-known Lotung site. The method was also applied to several CSMIP Geotechnical Arrays.

## Acknowledgment

The authors would like to acknowledge Prof. Pedro Arduino from the University of Washington for his fruitful comments, OpenSees implementation of the BA model, and Prof. Hamed Ebrahimain from the University of Nevada at Reno, who kindly shared his Bayesian estimation computer codes. The contributions of Dr. Wenyang Zhang and Dr. Fariba Abazarsa are greatly appreciated. The work presented in this manuscript was funded by the California Geological Survey (Contract No. 1019-015). Any opinions, findings, conclusions, or recommendations expressed in this material are those of the authors and do not necessarily reflect the views of the sponsoring agencies.

## References

[1] S. L. Kramer, *Geotechnical Earthquake Engineering*, vol. 6. New York: Prentice-Hall, 1996.

[2] I. M. Idriss and H. B. Seed, "Seismic Response of Horizontal Soil Layers," *J. Soil Mech. Found. Div.*, vol. 94, no. 4, pp. 1003–1034, 1968.

[3] J. M. Roesset, "Soil amplification of earthquakes," *Numer. methods Geotech. Eng.*, pp. 639–682, 1977.

[4] D. Park and Y. M. a. Hashash, "Soil Damping Formulation in Nonlinear Time Domain Site Response Analysis," *J. Earthq. Eng.*, vol. 8, no. 2, pp. 249–274, 2004, doi: 10.1080/13632460409350489.

[5] I. a Beresnev and K. Wen, "Nonlinear Soil Response-A Reality ?," *Bull. Seismol. Soc. Am.*, vol. 86, no. 6, pp. 1964–1978, 1996, doi: 10.1061/(ASCE)0733-9410(1996)122:9(725).

[6] E. H. Field and K. H. Jacob, "A comparison and test of various site-response estimation techniques, including three that are not reference-site dependent," *Bull. Seismol. Soc. Am.*, vol. 85, no. 4, pp. 1127–1143, 1995.

[7] A. W. Elgamal, M. Zeghal, H. T. Tang, and J. C. Stepp, "Lotung Downhole Array. I: Evaluation of Site Dynamic Properties," *J. Geotech. Eng.*, vol. 121, no. 4, pp. 350–362, 1995, doi: 10.1061/(ASCE)0733-9410(1995)121:4(350).

[8] S. F. Ghahari, F. Abazarsa, C. Jeong, A. Kurtulus, and E. Taciroglu, "Blind identification of site effects and bedrock motions from surface response signals," *Soil Dyn. Earthq. Eng.*, vol. 107c, pp. 322–331, 2018.

[9] S. F. Ghahari, F. Abazarsa, and E. Taciroglu, "Probabilistic blind identification of site effects from ground surface signals," *Bull. Earthq. Eng.*, 2017, doi: 10.1007/s10518-017-0253-0.

[10] J.-S. Lin, "Extraction of dynamic soil properties using extended Kalman filter," *J. Geotech. Eng.*, vol. 120, no. 12, 1994, doi: 10.1061/(ASCE)0733-9410(1994)120:12(2100).

[11] E. Şafak, "Models and methods to characterize site amplification from a pair of records," *Earthq. Spectra*, vol. 13, no. 1, pp. 97–129, 1997, doi: 10.1193/1.1585934.

[12] H. Ebrahimian, R. Astroza, J. P. Conte, and C. Papadimitriou, "Bayesian optimal estimation for output-only nonlinear system and damage identification of civil structures," *Struct. Control Heal. Monit.*, vol. 25, no. 4, 2018, doi: 10.1002/stc.2128.

[13] H. Ebrahimian, S. F. Ghahari, D. Asimaki, and E. Taciroglu, "A Nonlinear Model Inversion to Estimate Dynamic Soil Stiffness of Building Structures."

[14] C. Papadimitriou, J. L. Beck, and S. K. Au, "Entropy-based optimal sensor location for structural model updating," *JVC/Journal Vib. Control*, 2000, doi: 10.1177/107754630000600508.

[15] J. L. Beck and L. S. Katafygiotis, "Updating Models and Their Uncertainties. I: Bayesian Statistical Framework," *J. Eng. Mech.*, vol. 124, no. 4, pp. 455–461, 1998, doi: 10.1061/(ASCE)0733-9399(1998)124:4(455).

[16] C. McGann and P. Arduino, "Site response analysis of a layered soil column (total stress analysis)," *Opensees Ex. Wiki. Univ. Washingt.*, 2010.

[17] J. Lysmer and R. L. Kuhlemeyer, "Finite Dynamic Model For Infinite Media," *J. Eng. Mech. Div.*, vol. 95, no. 4, pp. 859–878, 1969, doi: 10.1089/dia.2007.0302.

[18] W. B. Joyner and A. T. F. Chen, "Calculation of nonlinear ground response in earthquakes," *Bull. Seismol. Soc. Am.*, vol. 65, no. 5, pp. 1315–1336, 1975.

[19] H. Ebrahimian, R. Astroza, J. P. Conte, and R. A. de Callafon, "Nonlinear finite element model updating for damage identification of civil structures using batch Bayesian estimation," *Mech. Syst. Signal Process.*, vol. 84, pp. 194–222, 2017, doi: 10.1016/j.ymssp.2016.02.002.

[20] S. Haykin, *Kalman Filtering and Neural Networks*, vol. 5, no. 3. 2001.

[21] S. J. Julier and J. K. Uhlmann, "New extension of the Kalman filter to nonlinear systems," in *Signal Processing, Sensor Fusion, and Target Recognition VI*, 1997, vol. 3068, p. 182, doi: 10.1117/12.280797.

[22] M. Vucetic and R. Dobry, "Effect of soil plasticity on cyclic response," *J. Geotech. Eng.*, 1991, doi: 10.1061/(ASCE)0733-9410(1991)117:1(89).

[23] R. I. Borja and A. P. Amies, "Multiaxial cyclic plasticity model for clays," *J. Geotech. Eng.*, vol. 120, no. 6, pp. 1051–1070, 1994.

[24] M. T. Manzari and Y. F. Dafalias, "A critical state two-surface plasticity model for sands," *Geotechnique*, 1997, doi: 10.1680/geot.1997.47.2.255.

[25] F. Pisanò and B. Jeremić, "Simulating stiffness degradation and damping in soils via a simple visco-elastic-plastic model," *Soil Dyn. Earthq. Eng.*, vol. 63, pp. 98–109, 2014, doi: 10.1016/j.soildyn.2014.02.014.

[26] Z. Yang, A. Elgamal, and E. Parra, "Computational Model for Cyclic Mobility and Associated Shear Deformation," *J. Geotech. Geoenvironmental Eng.*, vol. 129, no. 12, pp. 1119–1127, 2003, doi: 10.1061/(ASCE)1090-0241(2003)129:12(1119).

[27] D. C. Drucker and W. Prager, "Soil mechanics and plastic analysis or limit design," *Q. Appl. Math.*, vol. 10, no. 2, pp. 157–165, 1952, doi: 10.1090/qam/48291.

[28] F. McKenna, "OpenSees: a framework for earthquake engineering simulation," *Comput. Sci. Eng.*, vol. 13, no. 4, pp. 58–66, 2011.

[29] R. I. Borja, H. Y. Chao, F. J. Montans, and C. H. Lin, "Nonlinear ground response at Lotung LSST site," *J. Geotech. Geoenvironmental Eng.*, vol. 125, no. 3, pp. 187–197, 1999, doi: 10.1061/(ASCE)1090-0241(1999)125:3(187).

[30] M. B. Darendeli, "Development of a new family of normalized modulus reduction and material damping curves," 2001.

[31] M. Arduino, P; Taciroglu, E; Bonilla, F.; Taiebat, "Development of a numerical nonlinear soil module to expand the capabilities of the SCEC BroadBand Platform," 2019.

[32] R. L. Kuhlemeyer and J. Lysmer, "Finite element method accuracy for wave propagation problems," *J. Soil Mech. Found. Div.*, vol. 99, no. 5, pp. 421–427, 1973.

[33] H. T. Tang, Y. K. Tang, and J. C. Stepp, "Lotung large-scale seismic experiment and soil-structure interaction method validation," *Nucl. Eng. Des.*, 1990, doi: 10.1016/0029-5493(90)90260-5.

[34] X. S. Li, C. K. Shen, and Z. L. Wang, "Fully coupled inelastic site response analysis for 1986 Lotung earthquake," *J. Geotech. Geoenvironmental Eng.*, 1998, doi: 10.1061/(ASCE)1090-0241(1998)124:7(560).

[35] G. Elia, M. Rouainia, D. Karofyllakis, and Y. Guzel, "Modelling the nonlinear site response at the LSST down-hole accelerometer array in Lotung," *Soil Dyn. Earthq. Eng.*, 2017, doi: 10.1016/j.soildyn.2017.08.007.

[36] S. D. Glaser and L. G. Baise, "System identification estimation of soil properties at the Lotung site," *Soil Dyn. Earthq. Eng.*, 2000, doi: 10.1016/S0267-7261(00)00026-9.

[37] C. Y. Chang, C. M. Mok, and H. T. Tang, "Inference of dynamic shear modulus from Lotung downhole data," *J. Geotech. Eng.*, 1996, doi: 10.1061/(ASCE)0733-9410(1996)122:8(657).

[38] R. I. Borja, B. G. Duvernay, and C.-H. Lin, "Ground response in Lotung: total stress analyses and parametric studies," *J. Geotech. Geoenvironmental Eng.*, vol. 128, no. 1, pp. 54–63, 2002.

[39] M. Zeghal, A.-W. Elgamal, H. T. Tang, and J. C. Stepp, "Lotung Downhole Array. II: Evaluation of Soil Nonlinear Properties," *J. Geotech. Eng.*, vol. 121, no. 4, pp. 363–378, 1995, doi: 10.1061/(ASCE)0733-9410(1995)121:4(363).

[40] R. I. Borja, C. H. Lin, K. M. Sama, and G. M. Masada, "Modelling nonlinear ground response of non-liquefiable soils," *Earthq. Eng. Struct. Dyn.*, 2000, doi: 10.1002/(SICI)1096-9845(200001)29:1<63::AID-EQE901>3.0.CO;2-Y.

[41] M. Zeghal, A. W. Elgamal, H. T. Tang, and J. C. Stepp, "Lotung downhole array. II: Evaluation of nonlinear soil properties," *J. Geotech. Eng.*, 1995, doi: 10.1061/(ASCE)0733-9410(1995)121:4(363).

[42] Y. Tao and E. Rathje, "The Importance of Distinguishing Pseudoresonances and Outcrop Resonances in Downhole Array Data," *Bull. Seismol. Soc. Am.*, 2020, doi: 10.1785/0120190097.

[43] R. R. Ebrahimian, H.; Astroza, R.; Conte, J.P.; Bitmead, "An Information-theoretic Approach for Identifiability Assessment of Nonlinear Structural Finite Element Models," *ASCE J. Eng. Mech.*, vol. in press, 2018.

[44] E. Esmaeilzadeh Seylabi, E. Agapaki, D. Pitilakis, J. Stewart, S. Brandenberg, and E. Taciroglu, "Development of validated methods for soil-structure interaction analysis of buried structures," *Des. Dataset*, 2017.

[45] E. E. Seylabi, H. Ebrahimian, W. Zhang, D. Asimaki, and E. Taciroglu, "Bayesian Estimation of Nonlinear Soil Model Parameters Using Centrifuge Experimental Data," in *Geotechnical Special Publication*, 2018, doi: 10.1061/9780784481486.042.

[46] K. Afshari and J. Stewart, "Implications of California vertical array data for the analysis of site response with 1D geotechnical modeling," 2017.